μEDM Machining of ZrB_2-Based Ceramics Reinforced with SiC Fibres or Whiskers

Mariangela Quarto, Giuliano Bissacco, and Gianluca D'Urso

Abstract The effects of different reinforcement shapes on stability and repeatability of micro electrical discharge machining were experimentally investigated for Ultra-High Temperature Ceramics based on zirconium diboride (ZrB_2) doped by SiC. Two reinforcement shapes, namely SiC short fibres and SiC whiskers were selected in accordance with their potential effects on mechanical properties and oxidation performances. Specific sets of process parameters were defined minimizing the short circuits in order to identify the best combination for different pulse types. The obtained results were then correlated with the energy per single discharge and the discharges occurred for all the combinations of material and pulse type. The pulse characterization was performed by recording pulses data by means of an oscilloscope, while the surface characteristics were defined by a 3D reconstruction. The results indicated how reinforcement shapes affect the energy efficiency of the process and change the surface aspect.

Keywords micro-EDM · UHTCs · Ultra High Temperature Ceramics · Machinability

M. Quarto (✉) · G. D'Urso
Department of Management, Information and Production Engineering, University of Bergamo, Via Pasubio 7/b, 24044 Dalmine, BG, Italy
e-mail: mariangela.quarto@unibg.it

G. D'Urso
e-mail: gianluca.d-urso@unibg.it

G. Bissacco
Department of Mechanical Engineering, Technical University of Denmark, Produktionstorvet, Building 427, 2800 Kgs., Lyngby, Denmark
e-mail: gibi@mek.dtu.dk

E. Ceretti and T. Tolio (eds.), *Selected Topics in Manufacturing*,
Lecture Notes in Mechanical Engineering,
https://doi.org/10.1007/978-3-030-57729-2_5

1 Introduction

Among the advanced ceramic materials, Ultra-High-Temperature ceramics (UHTCs) are characterized by excellent performances in extreme environment. This family of materials is based on borides (ZrB_2, HfB_2), carbide (ZrC, HfC, TaC) and nitrides (HfN), which are characterized by high melting point, high hardness and good resistance to oxidation in several environments. In particular, ZrB_2-based materials are of particular interest because of their suitable properties combination and are considered promising for several applications; for example, among the most attractive applications, one is in the aerospace sector as a component for the re-entry vehicles and devices [1–4].

The relative density of the base material ZrB_2 is usually about 85% because of the high level of porosity of the structure; furthermore, in the last years, researchers are focused on fabricating high-density composites characterized by good strength (500–1000 MPa). For these reasons, the use of single-phase materials is not sufficient for high-temperature structural applications. Many efforts have been done on ZrB_2-based composites in order to improve the mechanical properties, oxidation performances, and fracture toughness; however, the low fracture toughness remains one of the greatest efforts for the application of these materials under severe conditions [5–10]. Usually, the fracture toughness of ceramic materials can be improved by incorporating appropriate reinforcements that activate toughening mechanisms such as phase transformation, crack pinning, and deflection. An example is the addition of SiC; in fact, it has been widely proved that its addition improves the fracture strength and the oxidation resistance of ZrB_2-based materials due to the grain refinement and the formation of a protective silica-based protective layer. Based on these aspects, the behaviour of ZrB_2-based composites, generated by the addition of SiC with different shapes (e.g. whiskers or fibres), have been studied in recent works. It has been reported that the addition of whiskers or fibres gives promising results, improving the fracture toughness and this improvement could be justified by crack deflection [5, 6, 9, 11, 12]. The critical aspect of the reinforced process was the reaction or the degeneration of the reinforcement during the sintering process itself [13, 14].

Despite all the studies that aim to improve mechanical properties and resistance, this group of materials is very difficult to machine by means of traditional technologies, because of their high hardness and fragility. Only two groups of processes are effective in processing them: on one side the abrasive processes as grinding, ultrasonic machining, and waterjet, on the other side the thermal processes such as laser and electrical discharges machining (EDM) [15–18].

In this work, ZrB_2 materials containing 20% vol. SiC whiskers or fibres produced by hot pressing were machined by the μEDM process; in particular, the effect of the non-reactive reinforcement shapes on the process performances were investigated, verifying if the process is stable and repeatable for advanced ceramics. The choice of 20% vol. is related to the evidence reported in some previous works [14, 18, 19], in which it was shown that this fraction of reinforcement allowed generating the

best combination of oxidation resistance and mechanical characteristics useful for obtaining better results in terms of process performances and dimensional accuracy for features machined by micro-EDM.

2 Materials

The following ZrB_2-based composites, provided by ISTEC-CNR of Faenza (Italy), were selected for evaluating the influence of reinforcement shape on the process performance of micro-slots machined by mEDM technology:

- ZrB_2 + 20% SiC short fibres, labelled as ZrB20f
- ZrB_2 + 20% SiC whiskers, labelled ZrB20w.

As reported by Silvestroni et al. [14], ZrB_2 Grade B (H.C. Starck, Goslar, Germany), SiC HI Nicalon-chopped short fibres, Si:C:O = 62:37:0.5, characterized by 15 μm diameter and 300 μm length or SiC whiskers characterized by average diameter 1 μm and average length 30 μm were used for the ceramic composites preparation.

The powder mixtures were ball milled for 24 h in pure ethanol using silicon carbide media. Subsequently, the slurries were dried in a rotary evaporator. Hot-pressing cycles were conducted in low vacuum (100 Pa) using an induction-heated graphite die with a uniaxial pressure of 30 MPa during the heating and were increased up to 50 MPa at 1700 °C (T_{MAX}), for the material containing fibres, and at 1650 °C (T_{MAX}) for the composites with whiskers. The maximum sintering temperature was set based on the shrinkage curve. Free cooling followed and details about the sintering runs are reported in Table 1, where T_{ON} identifies the temperature at which the shrinkage started. Density was estimated by the Archimedes method.

After the preparation, the raw materials were analysed by the Scanning Electron Microscope (SEM) (Fig. 1). The samples reinforced by the fibres show a very clear separation between the base matrix and the non-reactive reinforcement. Fibres dispersion into the matrix is homogenous and the fibres are characterized by the same orientation, as no agglomeration was observed in the sintered body. For the sample containing whiskers reinforcement, a dense microstructure was observed and the whiskers are generally well dispersed into the matrix. The SEM-EDS analysis

Table 1 Composition, sintering parameters of the hot-pressed samples [14]

Label	Composition	T_{ON} (°C)	T_{MAX} (°C)	Final density (g/cm^3)	Relative density (%)
ZrB20f	ZrB_2 + 20% SiC Short fibres	1545	1650	4.89	94.0
ZrB20w	ZrB_2 + 20% SiC Whiskers	1560	1700	5.22	97.0

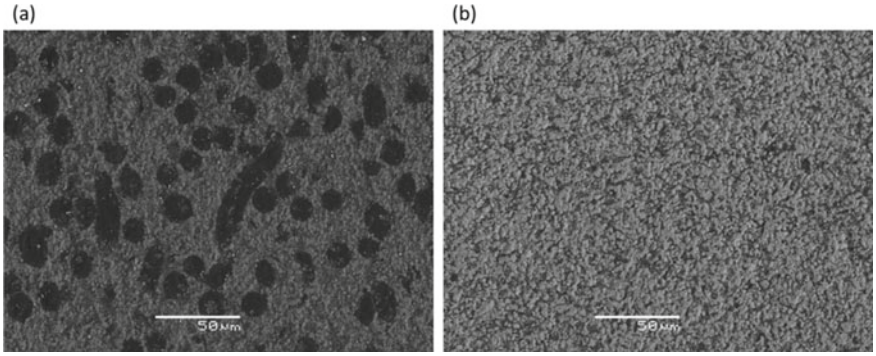

Fig. 1 SEM backscattered images of typical appearance of ZrB20f (**a**) and ZrB20w (**b**)

confirms these statements: for short fibres it is possible to observe a clear separation between the base matrix and the reinforcement. On the contrary, the analysis performed for samples containing whiskers shows that the two materials are mixed.

3 Electrical Discharge Machining Set-Up

3.1 Experimental Set-Up

The effects of selected reinforcement shapes were investigated by conducting μEDM milling experiments. A simple circular pocket having a diameter equal to 1 mm and a depth of about 200 μm was selected as the test feature. Solid tungsten carbide electrode with a diameter equal to 300 μm was used as a tool, and hydrocarbon oil was used as a dielectric fluid. The experiments were performed for three different process parameter settings, corresponding to different pulse shapes. The instantaneous values cannot be set for some process parameters, because the machine used for experiments presents an autoregulating system. Thus, the characterization of electrical discharges is very important, not only to assess the real value of process parameters but, most of all, to evaluate the stability and repeatability of the process. An acquisition system was developed and used to collect waveforms for characterizing the process. A current monitor with a bandwidth of 200 MHz and a voltage probe were connected to the μEDM machine and to a programmable counter and a digital oscilloscope (Rohde & Schwarz RTO1014). These connections allow to acquire the current waveforms and count the occurred discharges. The counter has been set once the trigger value was established to avoid recording and counting the background noise.

Preliminary tests were performed to define the optimal process parameters for each combination of material and pulse type. The experimental campaign was based on a general full factorial design, featured by two factors: the reinforcement shape, defined by two levels, and the pulse type, defined by three levels. Different levels of

pulse types identify the different duration of the discharges; in particular, level A is referred to long pulses while level C identify the short pulses. Three repetitions were performed for each run.

3.2 Discharge Population Characterization

Discharge populations were characterized by repeated waveform samples of current and voltage signals. The current and voltage probes were connected to the digital oscilloscope having a real-time sample rate of 40 MSa/s. The trigger level of the current signal was set to 0.5 A in order to acquire all the effective discharges avoiding the background noise. The acquired waveform samples were stored in the oscilloscope buffer and then transferred to a computer to be processed by a Matlab code, written by the authors and shown schematically in Fig. 2.

The Matlab code was used to calculate the numbers of electrical discharges, their instantaneous values, duration (width) and voltage. Finally, the average value of energy per discharge (E) was estimated by integrating the instantaneous value of the power, calculated as the product of the instantaneous values of current (i(t)) and voltage (v(t)), with respect to the time (t). In Fig. 3 the frequency distribution histograms show the discharge population distributions as a function of reinforcement shape and pulse type applied to the machining. Histograms show a good reproducibility and stability of the process, providing information regarding the frequency waveforms with different peaks of current. The normal distribution well represents the discharge samples which suggesting a stable process. Considering both reinforcement shapes, the intensities of the pulses are included in a similar range for pulses type A and B, while, for short pulse, they are characterized by some differences: for whiskers, the maximum peak current corresponds to the average value of the peaks occurred for the short fibres.

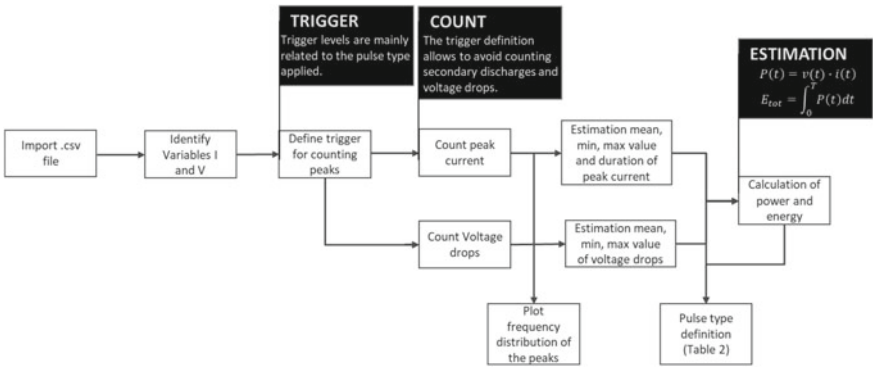

Fig. 2 Flowchart of Matlab code written by authors for the pulse characterization

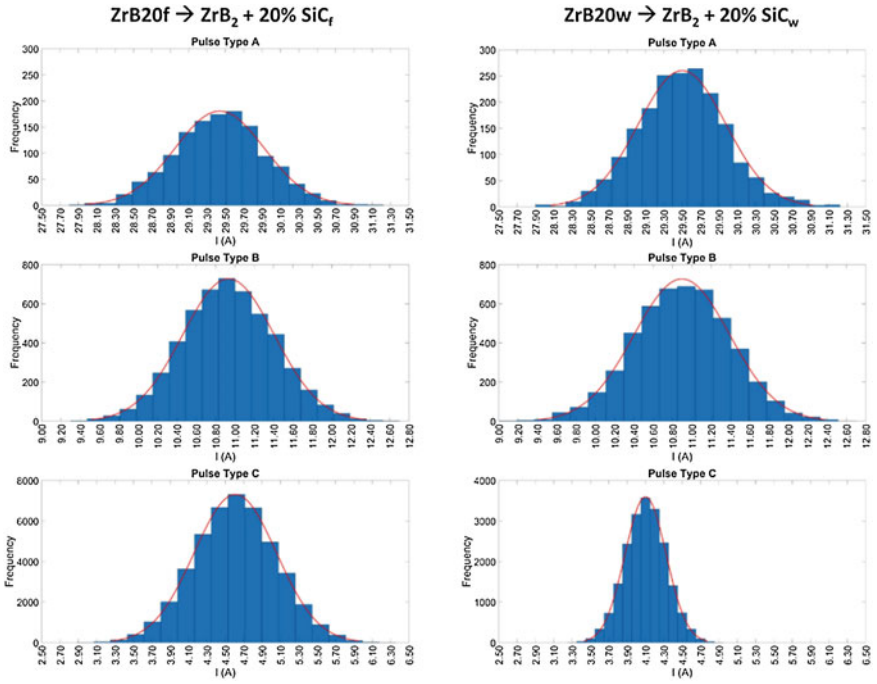

Fig. 3 Examples of frequency distribution histograms for pulses occurred during $ZrB_2 + 20\%SiC$ machining

$$E = \int_0^T v(t) \cdot i(t) dt \tag{1}$$

Through the Matlab data elaboration, it was possible to define the instantaneous value of the process parameters. The pulse characteristics for the estimated parameters are reported in Table 2.

Table 2 Mean values of the main parameters describing the pulse type

Reinforcement shape	Pulse type	Peak current (A)	Open circuit voltage (V)	Width (μs)	Energy per discharge (μJ)
Fibres (ZrB20f)	A	29.44	69.57	0.70	779.36
	B	10.93	92.89	0.33	150.30
	C	4.61	100.79	0.06	14.73
Whiskers (ZrB20w)	A	29.49	70.75	0.70	784.99
	B	10.91	91.70	0.33	161.00
	C	4.10	99.60	0.06	21.41

In terms of peaks of current and voltage, the differences between the two materials, machined by the same pulse type, are really tiny. The only relevant difference can be remarked for energy per discharge, in fact the discharges developed during the machining on the ZrB20w generate higher energy in comparison to the energy per discharge of ZrB20f. In particular, the energy per discharge generated by pulse type A for ZrB20w are 0.72% higher than the energy developed by the same pulse type for ZrB20f. This is a very tiny difference, but considering the pulse type C, the energy per discharge developed is about 45% higher than the energy generated by the same pulse type for fibres.

3.3 Characterization Procedure

A 3D reconstruction of micro-slots was performed by means of a confocal laser scanning microscope (Olympus LEXT) with a magnification of 20×. Then, the images were analysed with a scanning probe image processor software (SPIP by Image Metrology). A plane correction was performed on all the images to level the surfaces and to remove primary profiles; then, the surface roughness (Sa) was assessed by the real-topography method, based on the international standard UNI EN ISO 25178:2017. The process performance was evaluated through the estimation of two indicators related to the performance in terms of machining velocity and tool wear compared to the number of occurred discharges. The third indicator taken into account evaluates the tool wear ratio.

Material Removal per Discharge (MRD) was calculated as the ratio between the volume of micro-slots (MRW) estimated by the scanning probe image processor software and the number of discharges recorded by the programmable counter.

Since this kind of materials is characterized by high level of porosity, to get the actual values of MRD, the volume of the micro-slots was adjusted considering the relative density (δ) defined in Table 1. Taking into account the density allows compensating for the presence of porosity in the sample structure. Thus, the new indicator considered for the analysis was estimated as reported in (2).

$$MRD_{\delta} = MRD \cdot \delta \tag{2}$$

Tool Wear per Discharge (TWD) was estimated as the ratio between the volume of electrode wear (MRT) and the number of discharges recorded by the programmable counter. Tool wear was measured as the difference between the length of the electrode before and after the single milling machining. The length was measured through a touching procedure executed in a reference position. The electrode wear volume was estimated starting from the length of the tool wear and considering the tool as a cylindrical part. The Tool Wear Ratio (TWR) was calculated as the ratio between the previous performance indicators, considering the relative density of the workpiece material (TWR_{δ}) as reported in (3).

$$TWR_{\delta} = \frac{TWD}{MRD} = \frac{MRT}{MRW \cdot \delta} \tag{3}$$

4 Results and Discussion

In this section, the distribution of energy would be discussed, analysing the efficiency in terms of specific removal energy. Figure 4a shows the ratio between TWD and the energy of single discharge (TWD_E) as a function of the reinforcement fraction and the pulse type. In the same way, the MRD_{δ} was related to the energy of a single discharge to evaluate the energy efficiency from the material removed point of view. In both cases (Fig. 4a, b), pulse type A shows a lower efficiency; in other words, this means that most of energy developed in a single discharge was lost. This is a positive effect from the tool wear point of view; in fact, low TWD_E means low tool wear per discharge, and consequently a lowest tool wear. In this case, the pulse type C is characterized by a higher fraction of energy dedicated to the material removal from the workpiece, despite pulse type C is being characterized

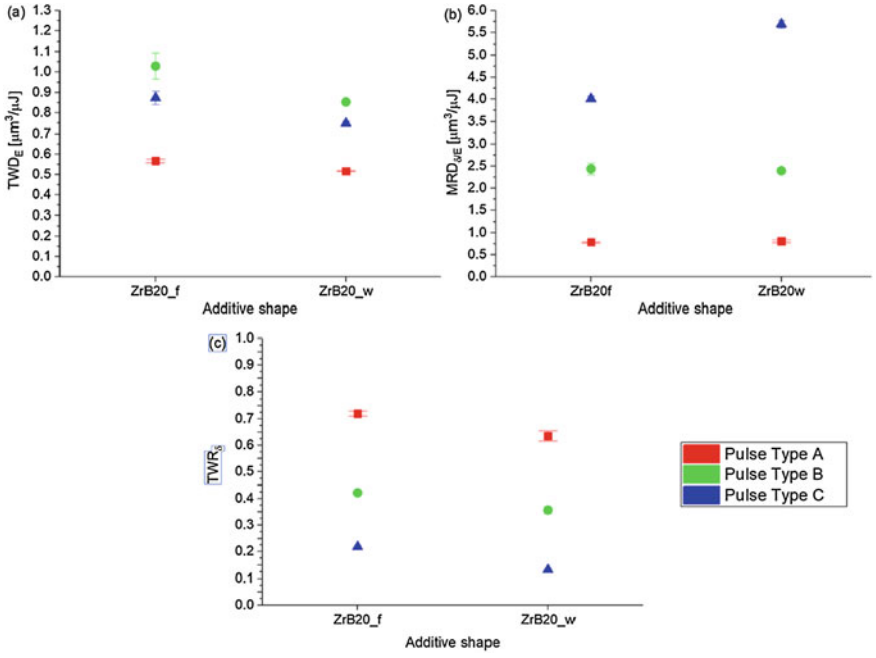

Fig. 4 Average values and standard deviation as a function of the reinforcement shape and pulse type, of **a** ratio between TWD and energy per discharge, estimated considering the relative density of the samples, **b** MRD and energy per discharge estimated considering the relative density of the samples, **c** TWR

Table 3 Analysis of variance *p*-values

		Factors		
		Pulse type	Reinforcement shape	Pulse type * reinforcement shape
Indicators	MRD_δ (μm^3)	0.000	1.21×10^{-4}	0.030
	TWD (μm^3)	0.000	0.000	4.51×10^{-5}
	TWRδ (–)	0.000	0.000	0.202
	Sa (μm)	0.000	0.005	0.156

by a very short duration and low energy (Fig. 4b). Despite the great difference in energy per discharge, this shows that the pulse type C directs most of the energy towards the workpiece. Figure 4c shows that the TWR for all pulse types is lower for specimens. In particular, the whiskers show a better performance allowing to reduce the tool wear and to increase the material removal rate efficiency. The intermediate position of pulse type C identified in Fig. 4a can be related to a different energy distribution. In particular, which energy fraction is dedicated to the material removal from the workpiece. The factorial design was analysed in order to comprehend which factors and interactions are statistically significant for the performance indicators and surface roughness. A general linear model was used to perform a univariate analysis of variance, including all the main factors and their interactions. The ANOVA results of the experimental plan are reported in Table 3. The parameters are statistically significant for the process when the *p*-value is less than 0.05 (a confidence interval of 95% is applied). As a general remark, all the indicators resulted to be influenced by both the reinforcement shape and the pulse type. In some cases (for MRD_δ and TWD), also the interaction showed an effect in terms of ANOVA. This aspect suggested that the interaction of factors is relevant for indicators that, in some way, can be correlated to the machining duration.

Main effects plots (Fig. 5) show that indicators are mainly influenced by the pulse type that establishes the range in which process parameters can vary, and in particular, the characteristics of the pulses. For all indicators, reduction in pulse duration and in peak current intensity generate the lower value of MRD_δ, TWD, and TWR_δ. At the same time, tests with whiskers reinforcement generate an improvement in MRD_δ and in surface finishing while giving rise to a reduction in TWD and TWR_δ. By increasing the pulse duration and the peak intensity from type C to type A, the MRD_δ is 10 times greater, but the surface quality decreases by −60%. For MRD_δ and TWD, also the interaction between pulse type and reinforcement shape affects the results. In particular, when the samples are machined by pulse type C, the effect on MRD_δ is more evident, while from the TWD point of view it is more evident for pulse type A (Fig. 6). In general, tests performed on materials with whiskers reinforcement are characterized by better results, both in terms of process performances and surface finishing. In fact, optimal performances for ED-machining are characterized by high level of MRD_δ, to perform fast machining, and low values of TWD, to reduce the waste of material related to the tool wear.

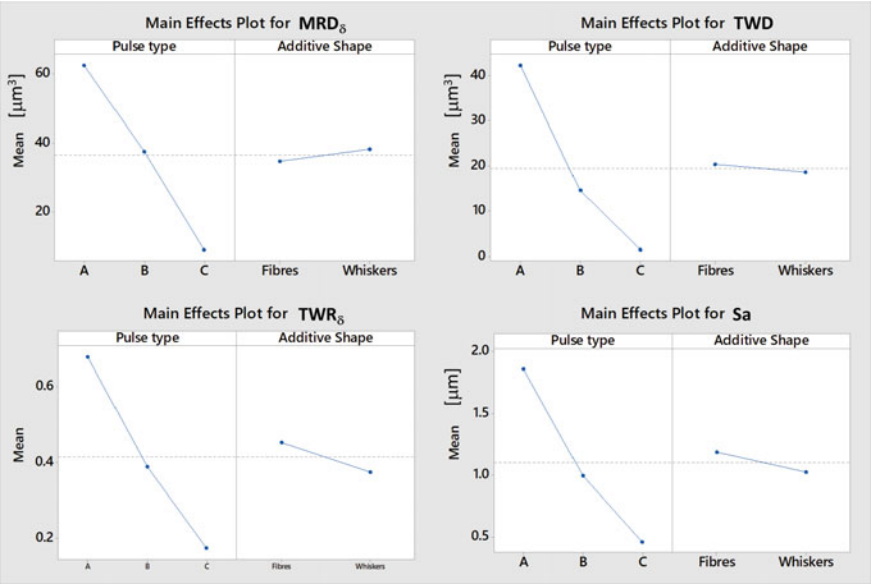

Fig. 5 Main effects plot for indicators affected by pulse type and reinforcement shape

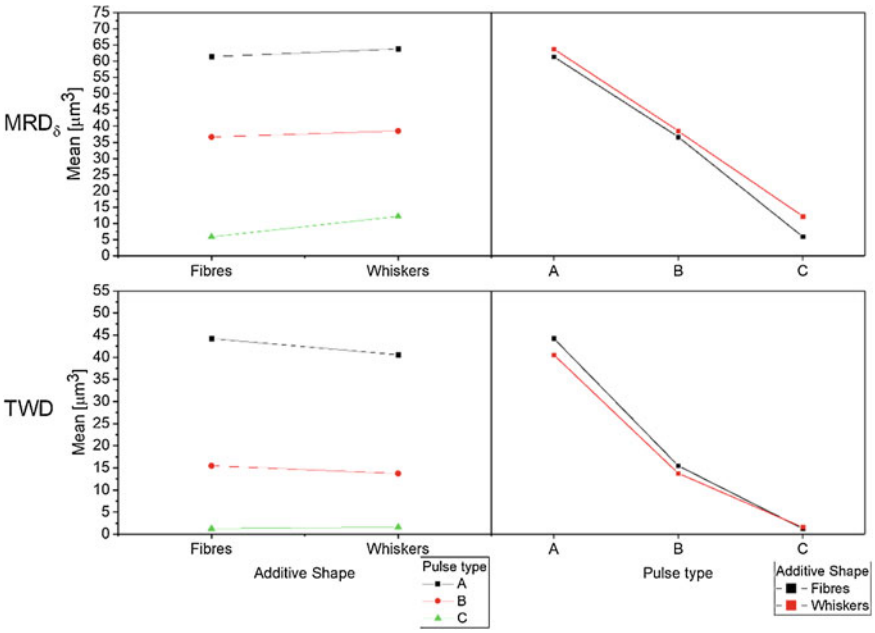

Fig. 6 Interaction plot for MRD_{δ} and TWD

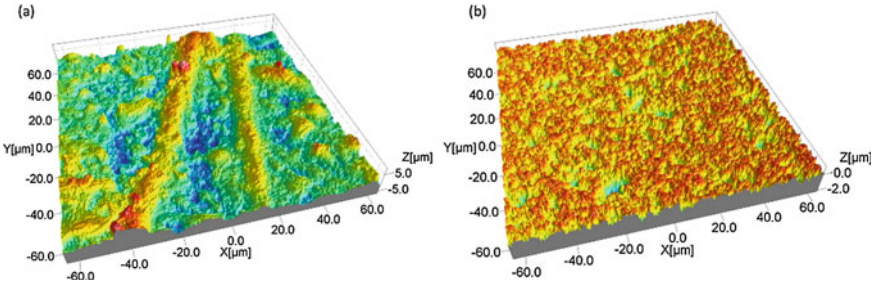

Fig. 7 Details of machined surfaces for ZrB20f (**a**) and ZrB20w (**b**) machined by pulse type A

A 3D reconstruction of an ED-machined surface detail scanned by a confocal laser scanning microscope with a magnification of 100× is reported as an example in Fig. 7. In particular, Fig. 7a represents a portion of the machined area on ZrB20f. Here it is possible to identify a sort of "protrusion" in correspondence of the fibres. This aspect is probably related to not complete machining because of the SiC low electrical conductivity characteristic and the great extension of the fibres area. Figure 7b represents the ED-machined surface for the sample containing SiC whiskers. In this case, the surface appears uniform and homogeneous because the SiC particles, as reported in the materials section, are better dispersed in the base matrix. These aspects justify the different results obtained in terms of surface quality and, in general, these different textures can be considered a starting point for further studies about the material removal mechanism occurred on UHTCs, in particular when there are low-electrically conductive parts in the structure. Form the 3D reconstruction it is possible to observe that the surfaces are not characterized by the typical aspect of the ED-machined surfaces which present a texture well-described by the presence of craters. In this specific case, the UHTC is different, but the same considerations can be done. A sort of craters can be observed by means of SEM (Fig. 8).

Machined surfaces on specimens doped with SiC whiskers are characterized by higher fragmentation of the recast layer. This aspect is particularly evident on surfaces machined by long pulses; in fact, for pulse type A and B, the surface is for the major part covered by recast materials for both reinforcement shapes, but the specimens doped with whiskers present smaller extensions of the single "crater" of recast materials.

A different behaviour can be observed for surfaces machined by the short pulses. In this case, for specimens containing the SiC fibres can be observed a smaller area of recast material, probably due to the combination of the greater dimensions of the fibres (in comparison to the whiskers), the lower energy per discharge for short pulses and the low electrical conductivity of the SiC. In particular, the fibres have a bigger surface and it needs to remove the entire parts. For this reason, the surfaces containing fibres presented in their correspondence a sort of protrusion.

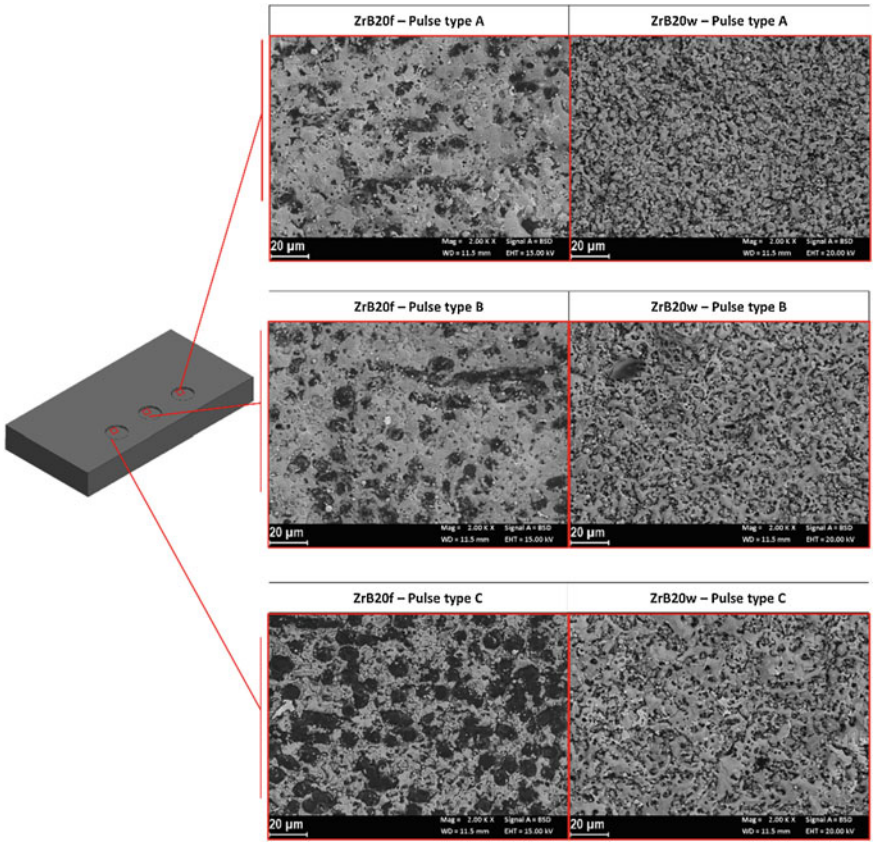

Fig. 8 SEM backscatter images of the machined surface

5 Conclusions

An evaluation of the machinability of ZrB_2-based composites hot-pressed with two different shapes non-reactive reinforcement (SiC) was performed in this work. Stability and repeatability of the µEDM were evaluated to identify the effects of the reinforcement shapes. The analysis took into account the process performances and surface finishing.

First of all, a discharge characterization was performed to feature the different pulse type used during the machining. In general, the discharge characterization and the performances indicators allowed to identify a stable and repeatable process with a faster material removal for samples doped with whiskers.

The analysis of variance showed that both factors, pulse type, and reinforcement shape, are statistically significant for the indicators selected in the process evaluation and in general, the use of whiskers improves the machining efficiency generating lower tool wear. Furthermore, the interaction between the two factors turns

out to be influential only for MRD and TWD, which are indirectly related to the machining duration, since the number of discharges occurred during the machining was considered in their estimation.

This investigation shows that the specimens having a 20 vol.% of reinforcement in form of whiskers results to be the best solution in terms of machinability by EDM process not only for the better process performances (high MRD and low TWD), but also for the higher level of surface quality which is one of the essential criteria for making a proper decision in an industrial environment.

Acknowledgements The authors would like to thank D. Sciti and L. Silvestroni from ISTEC—CNR of Faenza (Italy) for the production and supply of the materials used in this study.

References

1. Saccone G, Gardi R, Alfano D, Ferrigno A, Del Vecchio A (2016) Laboratory, on-ground and in-flight investigation of ultra high temperature ceramic composite materials. Aerosp Sci Technol 58:490–497
2. Upadhya K, Yang JM, Hoffman W (1997) Advanced materials for ultrahigh temperature structural applications above 2000 °C. Am Ceram Soc Bull 58:51–56
3. Levine SR, Opila EJ, Halbig MC, Kiser JD, Singh M, Salem JA (2002) Evaluation of ultra-high temperature ceramics for aeropropulsion use. J Eur Ceram Soc 22:2757–2767
4. Justin JF, Jankowiak A (2011) Ultra high temperature ceramics: densification, properties and thermal stability. AerospaceLab J 3:AL3-08
5. Zhang P, Hu P, Zhang X, Han J, Meng S (2009) Processing and characterization of ZrB_2-SiCW ultra-high temperature ceramics. J Alloys Compd 472:358–362
6. Wang H, Wang CA, Yao X, Fang D (2007) Processing and mechanical properties of zirconium diboride-based ceramics prepared by spark plasma sintering. J Am Ceram Soc 90:1992–1997
7. Zhang X, Xu L, Du S, Liu C, Han J, Han W (2008) Spark plasma sintering and hot pressing of ZrB_2-SiCW ultra-high temperature ceramics. J Alloys Compd 466:241–245
8. Zhang X, Xu L, Han W, Weng L, Han J, Du S (2009) Microstructure and properties of silicon carbide whisker reinforced zirconium diboride ultra-high temperature ceramics. Solid State Sci 11:156–161
9. Yang F, Zhang X, Han J, Du S (2008) Processing and mechanical properties of short carbon fibers toughened zirconium diboride-based ceramics. Mater Des 29:1817–1820
10. Yang F, Zhang X, Han J, Du S (2009) Characterization of hot-pressed short carbon fiber reinforced ZrB_2-SiC ultra-high temperature ceramic composites. J Alloys Compd 472:395–399
11. Zhang X, Xu L, Du S, Han J, Hu P, Han W (2008) Fabrication and mechanical properties of ZrB_2-SiCw ceramic matrix composite. Mater Lett 62:1058–1060
12. Tian WB, Kan YM, Zhang GJ, Wang PL (2008) Effect of carbon nanotubes on the properties of ZrB_2-SiC ceramics. Mater Sci Eng A 487:568–573
13. Guicciardi S, Silvestroni L, Nygren M, Sciti D (2010) Microstructure and toughening mechanisms in spark plasma-sintered ZrB_2 ceramics reinforced by SiC whiskers or SiC-chopped fibers. J Am Ceram Soc 93:2384–2391
14. Silvestroni L, Sciti D, Melandri C, Guicciardi S (2010) Toughened ZrB_2-based ceramics through SiC whisker or SiC chopped fiber additions. J Eur Ceram Soc 30:2155–2164
15. Rezaie A, Fahrenholtz WG, Hilmas GE (2013) The effect of a graphite addition on oxidation of ZrB_2-SiC in air at 1500 °C. J Eur Ceram Soc 33:413–421

16. Hwang SS, Vasiliev AL, Padture NP (2007) Improved processing and oxidation-resistance of ZrB_2 ultra-high temperature ceramics containing SiC nanodispersoids. Mater Sci Eng A 464:216–224
17. Zhang X, Liu R, Zhang X, Zhu Y, Sun W, Xiong X (2016) Densification and ablation behavior of ZrB_2 ceramic with SiC and/or Fe additives fabricated at 1600 and 1800 °C. Ceram Int 42:17074–17080
18. Zhang L, Kurokawa K (2016) Effect of SiC addition on oxidation behavior of ZrB_2 at 1273 K and 1473 K. Oxid Met 85:311–320
19. Sciti D, Guicciardi S, Silvestroni L (2011) SiC chopped fibers reinforced ZrB_2: effect of the sintering aid. Scr Mater 64:769–772